Published in: Molecular Physics

Quantum computation with vibrationally excited polyatomic molecules: effects of rotation, level structure, and field gradients

DANIEL WEIDINGER[1] and MARTIN GRUEBELE[1,2]

Departments of Physics[1], Chemistry[2], and Center for Biophysics and Computational Biology[2], University of Illinois, Urbana, IL 61801, USA

Abstract

Accurate rotation-vibration energy levels and transition dipoles of the molecule thiophosgene are used to model the execution of quantum gates with shaped laser pulses. Qubits are encoded in 2^n vibrational computing states on the ground electronic surface of the molecule. Computations are carried out by cycling amplitude between these computing states and a gateway state with a shaped laser pulse. The shaped pulse that performs the computation in the computing states is represented by a physical model of a 128-1024 channel pulse shaper. Pulse shapes are optimized with a standard genetic algorithm, yielding experimentally realizable computing pulses. We study the robustness of optimization as a function of the vibrational states selected, rotational level structure, additional vibrational levels not assigned to the computation, and compensation for laser power variation across a molecular ensemble.

1. Introduction

1.1. *Background*

Qubits can be represented by a quantum system in two fundamentally different ways. First, n qubits for quantum computation can be encoded in n separate degrees of freedom, often by a collection of two-level systems or quasi two-level systems[1-3]. When qubits are addressed directly in this manner, the challenge is how to entangle qubits that correspond to distinct or even spatially isolated degrees of freedom. Alternatively, $N = 2^n$ quantum states that may be non-degenerate can be used to represent qubit combinations [4]. This approach requires addressing a number of states that grows exponentially with the number of qubits, but has the utility that any combination of gates can be represented by a single $N \times N$ unitary transformation [5,6].

Both approaches have been studied using molecules. Individual modes of polyatomic molecules have been used to encode qubits [7-13]. Alternatively, series of vibrational states of diatomic molecules [5,14-16] or diatomic rotational-vibrational states [17] have been used to encode qubit combinations. In all of these studies, shaped laser fields are used to manipulate the coherence of molecular states to achieve quantum computation.

In either approach, molecules are an excellent testbed for studying effects of decoherence. For example, if only some degrees of freedom of a molecule are used for computation, coupling to others (unused vibrations or rotations) affects the desired phase relationships. Imperfections in laser pulses driving a molecular system, such as phase jitter, can also lead to loss of accuracy. A recent study by Zhao and Babikov examined such laser effects on vibrational wave packets used for quantum computing [18,19].

1.2. *Quantum computation in polyatomic molecules*

Here we study the effects of level structure, molecular rotation, and laser power inhomogeneity on quantum gates when qubit combinations are represented by a ladder of highly excited vibrational states.

Vibrationally excited polyatomic molecules offer both advantages and challenges for quantum computing via unitary transformations. A high density of states quasi-randomly distributed in energy is available for addressing the 2^n states representing qubit combinations. Unlike atomic or diatomic systems, polyatomic molecule angular momentum couplings are strongly quenched, and their rotational constants are very small. Effects such as rotational ladder climbing occur on time scales longer than the relevant vibrational time scale for quantum computation [20]. As is the case for atomic and diatomic systems, unwanted decoherence from thermal fluctuations is minimal because the energy scale $\Delta E_{vib} >> k_B T$ for vibrational states optically pumped in a cold (~ 5 K) molecular beam. Thus vibrational states not part of the 'computing states,' as well as rotational states can be used systematically to study decoherence effects.

Previous modeling encoding qubits in separate molecular modes used *ab initio* surfaces to build an accurate model of molecular vibrations [7,8,10]. The vibrational Hamiltonian and dipole surface of the molecule $SCCl_2$ (thiophosgene) are known accurately from experiment [21], so we study this molecule and use experimental data directly to build our Hamiltonian and dipole surface. Our computational approach differs from past work in one other significant way. We use a physical model of the pulse shaper to constrain the control pulse [22], instead of optimal control theory (OCT) [5,11]. Our model simulates in a straightforward manner experimental constraints on the laser pulse beyond a simple bound on fluence. The control pulse is optimized by a genetic algorithm [23] to perform quantum computations.

We study effects that potentially complicate the genetic algorithm optimization of the computing pulse, and which have received little attention in the literature so far: how the fidelity of pulses is affected by the states chosen for training in cases when perfect fidelity cannot be obtained [24]; how rotational ladder climbing in a polyatomic molecule reduces fidelity of the optimized pulse; how the energy distribution of vibrational states assigned as 'computing states' affects the optimization; how optimization is affected by the presence of unavoidable off-resonant states [6]; how it is affected by interspersed weak transitions not assigned to the computation; and how well optimized pulses work in the presence of laser power variations. (Phase variations have been discussed in detail by Zhao and Babikov [18].) Many of these factors are also important when complex physical systems other than molecules are to be controlled via unitary transformations. We conclude that shaped pulses applied to highly excited molecular vibrational states result in reasonably high fidelity operations in the presence of these complicating factors.

2. Methods

2.1. *Simulation parameters*

Figure 1 illustrates how a quantum computation is performed with vibrational levels on the ground electronic surface of thiophosgene. Anywhere from $N = 2$ to 16 vibrational levels are designated as computing states, and assigned to represent different qubit combinations $|\cdots 00\rangle$, $|\cdots 01\rangle$, $|\cdots 10\rangle$,$\cdots|\cdots 11\rangle$ (table 1). Table 1 shows accurate energy levels and transition dipoles for a contiguous set of 28 vibrational states from which computing states are selected.

To initialize the computation, a high resolution laser excites a single rotation-vibration state ($2^1 4^2$, $J = 0$) in the B' electronic manifold of the molecule to saturation. This initial state is the gateway state, and is well isolated from any other vibrational states. A Gaussian input pulse ($E_{max} = 10^9$ V/m) shaped by a pulse-shaper model then creates the initial superposition of computing states by dumping part of the gateway population down to the computing states on the ground electronic surface. The shaped pulse continues to cycle amplitude between the gateway state and the set of computing states (fig. 1).

The pulse computes by coherently manipulating the qubit amplitudes and phases through unitary time evolution under the Hamiltonian

$$H = H_{vib} - \mu\varepsilon(t) = H_{vib} - \sum_{j=1}^{J\le 21} \{|0><\mu_{0j}<j|\varepsilon(t)\} + \{|0><\mu_{0j}<j|\varepsilon(t)\}^{\dagger} . \quad (1)$$

Here H_{vib} is the vibrational Hamiltonian of thiophosgene, and μ_{0k} is the transition dipole operator between the single gateway state |0> and the manifold of vibrational states $\{|j>\}$.

2.2. *Propagation and optimization*

We use the SUR wavepacket propagator [25] to compute converged quantum dynamics of the vibrational wavepacket under eq. (1). SUR is a second order symplectic time propagator acting in the energy representation by matrix-vector multiplication, and offers a considerable speed advantage when numerous repetitive propagations of moderate accuracy need to be carried out [26]. The propagation includes states in the wings of the pulse, or states with small transition moment not assigned to the computation, because such states are unavoidable in real experimental applications.

Time evolution progresses until a target time t_f has been reached. Then a final transform-limited pulse pumps population to a single vibrational state in the $\tilde{A}^1A''$ electronic manifold of thiophosgene. Oscillations in the fluorescence of this state as a function of time delay ("quantum beats") read out the relative phases and amplitudes of the vibrational wave packet in the computing states.

In order for a meaningful computation to occur, the shaped pulse $\varepsilon(t)$ must be trained so that input states evolve to the desired output states via an optimized unitary transformation [6,27]. For example, consider a 2-qubit controlled-NOT (CNOT) gate, represented by the 4×4 matrix

$$\mathrm{CNOT} = \begin{pmatrix} 1 & 0 & 0 & 0 \\ 0 & 1 & 0 & 0 \\ 0 & 0 & 0 & 1 \\ 0 & 0 & 1 & 0 \end{pmatrix} . \quad (2)$$

Among four vibrational basis states |00>, |01>, |10> and |11>, this gate should map $|10>\rightarrow|11>$ for example; the gate flips the second qubit when the first "control" qubit is on.

To optimize a pulse for performing a gate such as eq. (2), we begin with an unshaped Gaussian pulse with $I(\omega) = I_0 \exp[-(\omega-\omega_0)^2/\Delta\omega^2]$, and compute a family of shaped pulses by applying a physical model of a pulse shaper. 'Physical model' means that the pulse shaper simulation can only phase-shift and attenuate the input pulse in the frequency domain over M = 128-1024 discrete channels [22], which is possible with electro-optic or liquid crystal pulse shapers. For each member of the pulse family, we calculate the fidelity of the computation – how accurately it represents a desired computation - as

$$F(t_f) = \frac{1}{K}\sum_{k=1}^{K}\left|\left\langle \psi_{\text{target,k}} \middle| \psi_k(t_f)\right\rangle\right|^2 . \quad (3)$$

F is the average overlap of the desired target state with each of K training input states Ψ_k propagated to t_f (analogous to the fidelity term in the OCT functional of [7]). A genetic algorithm is then used to optimize the pulse [23]. The fidelity would ideally reach unity, but will generally fall short of this goal for any gate sequence of significant complexity because of the constraints imposed on the pulse shaping, off-resonant excitation of non-computing states, etc.

The initial Gaussian pulse with a bandwidth-duration product of $\omega_P\ t_P = 0.441$ is stretched from 100 fs up to 5-50 ps by this process, depending on the number of pulse shaper channels. To simulate the final readout, we average phases and amplitudes over a window of duration t_P, as would occur with a transform-limited readout pulse. The maximum pulse stretching/readout time is given by $t_f / t_P \sim M$ if the pulse fills the shaper. This defines the maximum information entropy $S_P \sim \ln M$ of the pulse.

3. Results

3.1. *Simple gates*

Simulations implemented the basic computationally complete set of gates [28], represented by the matrices

$$\text{Hadamard} = \frac{1}{\sqrt{2}}\begin{pmatrix} 1 & 1 \\ 1 & -1 \end{pmatrix}, \quad \text{phase} = \begin{pmatrix} 1 & 0 \\ 0 & e^{i\varphi} \end{pmatrix} \quad (4)$$

and the CNOT gate in eq. (2). Figure 2 shows the result, using 2 to 4 of the thiophosgene vibrational states in table 1 as computing states. Fidelities over 95% were achieved with fewer than 1000 iterations of the genetic algorithm, despite the presence of non-computing states at lower and higher energies (figure 1).

The fidelity is smoother for two qubits (compare the CNOT vs. single qubit traces in figure 2). Two phenomena account for this. Firstly, the more energy levels are accessible to the pulse, the more population fluctuations in the excited state gateway level are reduced and high-frequency oscillations (quantum beats) in the fidelity are dampened. Secondly, for smaller numbers of qubits, the optimized pulse is more likely to cycle population several times before steering it into the correct state at t_f. One could design against such unnecessary cycling, but this is not a problem for more complex gates.

3.2. *Training set dependence of the fidelity*

The pulse is optimized for a finite number of input cases $K \geq N = 2^n$. Ideally, the pulse performs the computation for any untrained input, once N linearly independent inputs are mapped exactly to the desired outputs. Because the fidelity does not necessarily reach unity, we must ask how large K needs to be so the optimized pulse works well for all untrained inputs. Our

criterion for successful training was that the resulting pulse should have the same operator fidelity, whether it is applied to the training set, or to a completely different set of randomly chosen input vectors. We found that for two-level gates such as the NOT or phase gate, the smallest training basis {|0>, |1>} is sufficient.

For gates of four or more levels it is necessary to augment the basis set with additional linearly dependent input vectors. However, the set required to obtain good performance is not very large. Consider the case of the four-level gate CNOT. When training with only the four minimal basis vectors {|00>, ··· |11>}, greater than 99% fidelity was achieved during training, but less than 80% for other randomly chosen inputs. In this case, we find that it is advantageous to augment the training set with an input vector that contains a superposition of states. A training map augmented by just one more input (still an unentangled qubit combination)

$$\begin{pmatrix}1\\0\\0\\0\end{pmatrix},\begin{pmatrix}0\\1\\0\\0\end{pmatrix},\begin{pmatrix}0\\0\\1\\0\end{pmatrix},\begin{pmatrix}0\\0\\0\\1\end{pmatrix},\frac{1}{2}\begin{pmatrix}1\\1\\1\\1\end{pmatrix} \tag{5}$$

resulted in a trained pulse with a fidelity of 99%, as good as the smaller training set. The same pulse executes the three untrained maps (A and B are entangled)

$$|A\rangle = \frac{1}{\sqrt{2}}\begin{pmatrix}0\\1\\-1\\0\end{pmatrix} \to \frac{1}{\sqrt{2}}\begin{pmatrix}0\\1\\0\\-1\end{pmatrix},\quad |B\rangle = \frac{1}{\sqrt{2}}\begin{pmatrix}-1\\0\\0\\1\end{pmatrix} \to \frac{1}{\sqrt{2}}\begin{pmatrix}-1\\0\\1\\0\end{pmatrix},\quad |C\rangle = \frac{1}{\sqrt{2}}\begin{pmatrix}0\\0\\-i\\1\end{pmatrix} \to \frac{1}{\sqrt{2}}\begin{pmatrix}0\\0\\1\\-i\end{pmatrix} \tag{6}$$

with > 95% fidelity as shown in figure 3. We found that good performance on randomly chosen input states requires training sets sampling highly filled superpositions of vibrational states in addition to the minimal basis, as in eq. (5). We also observed large improvements for 3 and 4 qubit transformations whenever a few highly filled states were added to the minimal training set.

3.3. *Scaling of more complex gates*

A nontrivial test of laser control of polyatomic vibrations is its capacity to implement Shor's Algorithm equally as well as simpler 4-qubit transformations. This would support the claim that once a given number of qubits is implemented, all transformations are about equally hard. Figure 4 shows the time evolution of the optimal fidelity for an already extensively studied 16-level version of the phase estimation procedure from the algorithm to factor 15 [28]. Table 1 shows how the 16 required basis functions were assigned to vibrational energy levels. The algorithm is summarized by the following circuit diagram (read right to left), following the work of Beckman [29]:

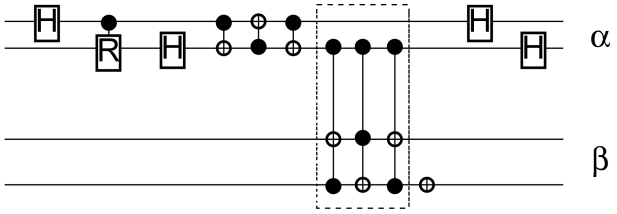

(7)

Scheme (7) uses standard notation where H denotes a Hadamard transform, black/white circles controlling/controlled bits of CNOT gates, and R a $\pi/2$ controlled phase gate. In matrix form, this algorithm becomes

$$\mathrm{SHOR} = \frac{1}{2}\begin{pmatrix}
0 & 2 & 0 & 0 & 0 & 0 & 0 & 0 & 0 & 0 & 0 & 0 & 0 & 0 & 0 & 0 \\
1 & 0 & 0 & 1 & 1 & 0 & 0 & -1 & 0 & 0 & 0 & 0 & 0 & 0 & 0 & 0 \\
1 & 0 & 0 & 1 & -1 & 0 & 0 & 1 & 0 & 0 & 0 & 0 & 0 & 0 & 0 & 0 \\
0 & 0 & 2 & 0 & 0 & 0 & 0 & 0 & 0 & 0 & 0 & 0 & 0 & 0 & 0 & 0 \\
0 & 0 & 0 & 0 & 0 & 0 & 0 & 0 & 1+i & 0 & 0 & 0 & 0 & 1-i & 0 & 0 \\
0 & 0 & 0 & 0 & 0 & 0 & 0 & i & 0 & 0 & 0 & i & 1 & 0 & 0 & -i \\
0 & 0 & 0 & 0 & 0 & 0 & 0 & 0 & 0 & 0 & 0 & 1 & -i & 0 & 0 & 1 \\
0 & 0 & 0 & 0 & 0 & 0 & 0 & 0 & 0 & 0 & 1+i & 0 & 0 & 0 & 1-i & 0 \\
0 & 0 & 0 & 0 & 0 & 2 & 0 & 0 & 0 & 0 & 0 & 0 & 0 & 0 & 0 & 0 \\
1 & 0 & 0 & -1 & 1 & 0 & 0 & 1 & 0 & 0 & 0 & 0 & 0 & 0 & 0 & 0 \\
-1 & 0 & 0 & 1 & 1 & 0 & 0 & 1 & 0 & 0 & 0 & 0 & 0 & 0 & 0 & 0 \\
0 & 0 & 0 & 0 & 0 & 0 & 2 & 0 & 0 & 0 & 0 & 0 & 0 & 0 & 0 & 0 \\
0 & 0 & 0 & 0 & 0 & 0 & 0 & 0 & 0 & 1-i & 0 & 0 & 0 & 1+i & 0 & 0 \\
0 & 0 & 0 & 0 & 0 & 0 & 0 & 0 & 1 & 0 & 0 & -i & 1 & 0 & 0 & i \\
0 & 0 & 0 & 0 & 0 & 0 & 0 & 0 & -i & 0 & 0 & 1 & i & 0 & 0 & 1 \\
0 & 0 & 0 & 0 & 0 & 0 & 0 & 0 & 0 & 0 & 1-i & 0 & 0 & 0 & 1+i & 0
\end{pmatrix} \tag{8}$$

Figure 4 demonstrates that level spacing and dipole fluctuations as they occur in a real polyatomic molecule do not present a problem for optimizing the computing pulse. Most importantly SHOR is implemented nearly as accurately (> 90% fidelity) as the simpler U_{654} gate also indicated in eq. (7) by a dashed box.

To make this more quantitative, we define an information entropy $S_{op}(N, R)$ of a quantum computation operator as a function of its size and off-diagonality R.[†] By equating S_P and S_{op}, and determining the value M required for several different quantum computations to have a fidelity halfway between the minimum (unshaped pulse) and 1, we obtain the empirical relationship

$$S_{op} \approx a \ln(1 + 2^n R^b) \text{ with } a \approx 1.2, b \approx 0.25 . \tag{9}$$

Consider the scaling of S_{op} with size $N = 2^n$ first. As expected, $S_{op} \sim n$ nearly holds [6], so the number of pixels M necessary for a typical (partially but not fully off-diagonal) operator grows nearly linearly with N. In the case of a 2-level NOT gate, an optimized 8-pixel array is sufficient for >99% fidelity, while the 4-level CNOT (see eq. 6) does not attain such a high fidelity unless $M \geq 32$. Optimizations with M = 256-512 were necessary to reach half-way fidelities with the U_{654} and SHOR gates. S_{op} depends only weakly on R, so how filled-in the operator matrix is has only secondary importance.

[†] R is defined as the number of flip/add operations required to obtain the operator from the identity operator. The identity operator, no matter how many qubits it transforms, can be implemented without any pulse, so $S_I = 0$ always. The "1+" factor is added to our empirical scaling relationship to produce the correct behavior when the identity is approached.

3.4. *Laser power effects*

In real applications, laser peak power varies across the laser beam profile. The effective power also varies because molecular orientation decreases the projection of the electric field along the transition dipole axis, and laser amplitude noise is usually present. Presumably, these problems could be corrected by spatially shaping the beam profile with a phase mask or deformable mirror, and by orienting the molecules somehow. It would be much more economical if one could simply design pulse shapes to optimize fidelity independently of laser power. Rabitz and coworkers discuss an existence theorem for pulse shapes that optimize a given control process at multiple laser intensities [30,31]. We thus addressed the power issue by simultaneously optimizing at different average intensities for each pulse shape. Using only three different field values for training cases (100%-75%-50%), a pulse mask for CNOT was generated, capable of performing the same operation at all laser power down to less than 40% of the maximum in the center of the beam, with less than 10% fidelity variation (figure 5). Using a denser set of the training laser intensities improved the fidelities of the intermediate cases, with a cost increase linear in the number of cases.

3.5. *Rotational angular momentum*

In diatomic molecules, the inclusion of rotational degrees of freedom in the Hamiltonian can significantly alter the shape of an optimized laser pulse, although it has been shown that control is still possible [32]. The main advantage of quantum computing with heavy polyatomic molecules over atoms or diatomic molecules is their high mass and low symmetry, which reduces the effects of angular momentum couplings. The largest effect in $SCCl_2$ is rotational ladder climbing in the rigid rotor approximation. Each vibrational state, treated as a single energy level so far, in fact contains a multitude of rotational levels characterized by quantum numbers J (total angular momentum), K_A and K_c (projection of J onto the axes of smallest and largest moment of inertia) and M_J (space-fixed projection of J). As the molecule is shuttled back-and-forth between the gateway and computing states, the selection rules populate states with successively higher J. This washes out the coherence over a finite energy range. We treat this problem based on the rigid rotor, asymmetric top Hamiltonian H_{RR} in wavenumber units [33]

$$\{H_{RR} / hc\} \mid JK_aK_cM_J >= \{AJ_a^2 + BJ_b^2 + CJ_c^2\} \mid JK_aK_cM_J > \qquad (10)$$

The rotational constants A, B and C are half the inverse principal moments of inertia in wavenumber units. For the ground electronic state of thiophosgene containing the computing states, they are A=0.119 cm^{-1}, B=0.116 cm^{-1} and C=0.059 cm^{-1}; for the B^1 excited electronic state containing the gateway state, they are A=0.139 cm^{-1}, B=0.084 cm^{-1} and C=0.052 cm^{-1} {Strickler, 2001 #837; Bigwood, 1998 #203}.

The next largest effects involve rotation-vibration and Coriolis couplings. The rotation-vibration term in the Hamiltonian is smaller by the unitless scaling parameter $3\bar{\alpha}/(A+B+C) \approx 0.01$. Here $\bar{\alpha}$ is the average correction to the rotational constants of eq. (5) caused by vibrational excitation. Usually vibrational motion increases the size of a molecule, thus lowering the rotational constants. The Coriolis correction to the energy is smaller by the unitless Coriolis coupling parameter $\zeta \approx 0.1$ {Gruebele, 2004 #926}. This correction arises because vibrations lag in the rotating frame of the molecule, much as a ball aimed at a person on a merry-go-round will deviate from its target, which is rotating away from the original aim. These lead to much slower drifts in the relative phases of states, and we neglect them here.

Using A'→A' symmetry selection rules for the electronic transition from ground state to B^0 state, we computed energy levels for eq. (10) and transition moments for all $|JK_aK_cM_J>$ states with $J \leq 5$ to model up to 5 cycles of ladder climbing, the most expected for vibrational quantum computation with thiophosgene at the laser input power used here ($\leq 10^9$ V/m). We then re-optimized the CNOT pulse, assuming an initial gateway rotational state |0000>, which can indeed be prepared using a high resolution laser. The resulting fidelity is shown in figure 6. At the end of the computation, the population in the $J = 5$ levels was still small compared to lower J values. A fidelity > 0.95 was again obtained for the CNOT gate with ro-vibrational levels.

3.6. *Interference from additional states*

As shown in figure 1, non-computing vibrational states usually lie just outside the energy range spanned by computing states [6]. The probability of finding a group of 2^n states nicely clustered with no other states nearby is small. To examine how such states affect the fidelity of quantum gates, we repeated the optimization of the gates in figures 2 and 4 with only the computing states included. Only the gates of figure 2(d) and figure 6 showed significant improvement (each increased about 3% in fidelity), and no significant decrease of the pulse complexity was evident by visual inspection of the windowed Fourier transform. Thus optimization can deal with states outside the computing window successfully.

A complex spectrum will also have states with weak transition moments interspersed among stronger transitions. As a worst-case scenario, table 1 shows 4-qubit combinations reassigned from weaker transitions at maximum input pulse power to stronger transitions in the wings of the pulse. The resulting SHOR algorithm fidelity dropped by 14%. However, the ratio of strong to weak dipole magnitudes was at most 3:1 in this calculation. For the CNOT gate, once the omitted states have dipole × field products < 0.1 of the strongest transitions, no significant deterioration of the optimization occurred.

4. Discussion

Vibrationally excited polyatomic molecules have a greater number of easily addressable states as a basis for quantum computing than do diatomics or atoms. The long (usually > μs) radiative lifetime makes well-defined coherent excitation of state superpositions easy. However, polyatomic molecules, as well as other complex quantum systems, pose their own challenges for robust control. Their rotational structure is complex, although the rotational constants are at least small. States with small transition moments may be interspersed with states assigned to a computational basis. Other states lie outside the computational bandwidth, but can still be excited and withdraw population from the computing states. It may not be possible to achieve 100% fidelity for the minimal set of 2^n independent input states, raising the question of whether training can be improved by augmenting the training basis. For computations using optical excitation, there are several sources of laser power variation, requiring a given computing pulse shape to work well over a range of average powers. A study of these effects is of interest not just for control of polyatomic molecules, as they can also play a role when other complex quantum systems are used in quantum computation.

We find that polyatomic vibrational levels encoding 2^n qubits can be coherently manipulated to perform quantum computation tasks, even in the presence of laser power variation across the beam profile, rotational level structure, or additional vibrational states not assigned to represent qubit combinations. The effect of phase jitter has been considered in detail earlier [18]. We find that transitions whose product of transition dipole magnitude and input field magnitude is less than about one tenth of the strongest transitions need not be assigned as computing states. Training is robust with small training sets that have been augmented only by a few filled-in states, i.e. those simultaneously populating many vibrational levels. Such states help lock the phase relationship between different vibrational levels contributing to $\Psi_k(t)$ [24].

How qubit combinations are encoded in vibrational states could have an effect on the robustness of the computation or complexity of the control field. We have made the most obvious assignment, ascending or descending in energy, as shown below eq. (2) or in table 1. However, we could have walked through the control bit first, i.e. |0> = |00>, |1> = |10>, |2> = |01> and |3> = |11>, flipping the states |1> and |2>. Fidelities greater than 99% were obtained for both qubit assignments, but significantly different paths were taken to the target state. In the second scheme, more population is cycled through gateway states and the resulting trained pulse is more complex. As one might expect, qubits that tend to be transformed together should be grouped together during encoding.

The results shown in figures 2 and 4 correspond to an optimal selection of the 2-16 vibrational states assigned to qubit combinations. This raises the issue of how much the fidelity fluctuates as the center frequency of the pulse to be trained is scanned across the vibrational spectrum. Figure 7 shows the variation in fidelity obtained for the CNOT gate. Successive groups of four vibrational states were selected to represent 2 qubits, and the center frequency of

the pulse to be trained was placed at their average transition frequency. The pulse was then trained using the training set of eq. (5). The fidelity varied by up to 20%, indicating that finding the optimal location in the vibrational spectrum is helpful, but that the variations are not enormous.

5. Conclusion

Even when there is leakage of amplitude into weak transitions, and rotational level structure is included, small training sets can provide robust pulses operating over a wide range of average powers to implement quantum computations from basic gates to prime factorization using 2^n vibrational states of a polyatomic molecule to encode n qubits. This was shown using a realistic molecular Hamiltonian and dipole surface.

This work was supported by the National Science Foundation. DW was supported by a grant from the UIUC Research Board.

References

[1] GERSHENFELD, N. A., CHUANG, I. L., 1997, *Science,* **275,** 350.

[2] AVERIN, D. V., 2000, *Progr. of Physics,* **48,** 1055.

[3] KWIAT, P., MITCHELL, J., SCHWINDT, P., WHITE, A., 2000, *J. Modern Optics,* **47,** 257.

[4] AHN, J., WEINACHT, T. C., BUCKSBAUM, P. H., 2000, *Science,* **287,** 463.

[5] PALAO, J. P., KOSLOFF, R., 2002, *Physical Review Letters,* **89,** 188301.

[6] PALAO, J. P., KOSLOFF, R., 2003, *Physical Review A,* **68,** 062308.

[7] TESCH, C. M., VIVIE-RIEDLE, R. D., 2002, *Phys. Rev. Lett.,* **89,** 157901.

[8] KORFF, B. M. R., TROPPMANN, U., KOMPA, K. L., VIVIE-RIEDLE, R. D., 2005, *J. Chem. Phys.,* **123,** 244509.

[9] TROPPMANN, U., VIVIE-RIEDLE, R. D., 2005, *J. Chem. Phys.,* **122,** 154105.

[10] TROPPMANN, U., GOLLUB, C., DE VIVIE-RIEDLE, R., 2006, *New Journal of Physics,* **8,** 100.

[11] TESCH, C. M., KURTZ, L., VIVIE-RIEDLE, R. D., 2001, *Chemical Physics Letters,* **343,** 633.

[12] AMITAY, Z., KOSLOFF, R., LEONE, S. R., 2002, *Chemical Physics Letters,* **359,** 8.

[13] BABIKOV, D., 2004, *Journal of Chemical Physics,* **121,** 7577.

[14] VALA, J., AMITAY, Z., ZHANG, B., LEONE, S. R., KOSLOFF, R., 2002, *Physical Review A,* **66,** 062316.

[15] OHTSUKI, Y., 2005, *Chemical Physics Letters,* **404,** 126.

[16] TERANISHI, Y., OHTSUKI, Y., HOSAKA, K., CHIBA, H., KATSUKI, H., OHMORI, K., 2006, *Journal of Chemical Physics,* **124,** 114110.

[17] SHAPIRO, E. A., KHAVKINE, I., SPANNER, M., IVANOV, M. Y., 2003, *Physical Review A,* **67,** 013406.

[18] ZHAO, M. Y., BABIKOV, D., 2006, *Journal of Chemical Physics,* **125,** 024105.

[19] ZHAO, M. A. B., DMITRI, 2007, *The Journal of Chemical Physics,* **126**.

[20] GRUEBELE, M., 2004, *J. Phys. : Condens. Matter,* **16,** R1057.

[21] STRICKLER, B., GRUEBELE, M., 2004, *Phys. Chem. Chem. Phys.,* **6,** 3786.

[22] BIGWOOD, R. M., GRUEBELE, M., 2002, *J. Mol. Struct. (Theochem),* **589,** 447.

[23] GOLDBERG, D. E.: Genetic Algorithms, Addison-Wesley, New York, 1989.

[24] TESCH, C. M., DE VIVIE-RIEDLE, R., 2004, *Journal of Chemical Physics,* **121,** 12158.

[25] BIGWOOD, R., GRUEBELE, M., 1995, *Chem. Phys. Lett.,* **233,** 383.

[26] ENGEL, M., GRUEBELE, M., 2006, *Chem. Phys. Lett.,* **433,** 368.

[27] RANGAN, C., BUCKSBAUM, P. H., 2001, *Phys. Rev. A,* **64,** 033417.

[28] NIELSEN, M. A., CHUANG, I. L.: Quantum Computation and Quantum Information, Cambridge University Press, Cambridge, 2000.

[29] BECKMAN, D., CHARI, A. N., DEVABHAKTUNI, S., PRESKILL, J., 1996, *Phys. Rev. A,* **54,** 1034.

[30] SUNDERMANN, K., RABITZ, H., VIVIE-RIEDLE, R. D., 2000, *Physical Review A,* **62,** 013409.

[31] HO, T. S., RABITZ, H., 2006, *Journal of Photochemistry and Photobiology a-Chemistry,* **180,** 226.

[32] HORNUNG, T., DE VIVIE-RIEDLE, R., 2003, *Europhys. Lett.,* **64,** 703.

[33] PAPOUSEK, D., ALIEV, M. R.: Molecular Vibrational-Rotational Spectra, Elsevier, Amsterdam, 1982.

Tables

Table 1: Vibrational energy levels and transition dipole moments derived from ref. [21]. The qubit assignments used in figures 2 to 6 are shown.

Wavenumber (cm^{-1})	μ (Debye)	2-qubit assg. CNOT	4-qubit assg. SHOR	SHOR reassigned
8032.86	0.47			
8067.17	0.41			
8080.09	0.96			|0000>
8087.79	0.94			
8101.18	1.00			|0001>
8111.49	0.44			
8126.73	0.42		|0000>	|0010>
8136.98	0.96		|0001>	|0011>
8182.75	0.55		|0010>	|0100>
8191.03	0.44		|0011>	
8239.53	0.36		|0100>	
8246.35	0.38	|00>	|0101>	|0101>
8264.26	0.96	|01>	|0110>	|0110>
8273.98	0.75	|10>	|0111>	
8278.82	0.70	|11>	|1000>	
8292.89	0.61		|1001>	|0111>
8319.93	0.43		|1010>	|1000>
8342.37	0.62		|1011>	|1001>
8366.49	0.62		|1100>	|1010>
8372.81	0.54		|1101>	
8398.00	0.53		|1110>	|1011>
8414.60	0.29		|1111>	|1100>
8427.80	1.00			|1101>
8444.25	0.29			
8457.20	0.42			|1110>
8471.08	0.26			
8481.07	0.84			|1111>
8492.72	0.42			

Figure captions

Figure 1: (Web color) The arrows illustrate the computing pulse sequence. From a jet-cooled ground state distribution, a pure gateway state in the $\tilde{B}$ electronic state ($v_1 = 1$, $J = 0$, $K_A = 0$, $K_C = 0$) is excited by a high resolution laser at 35125 cm^{-1}. This gateway is separated by at least ±100 cm^{-1} from other vibrational states. A shaped pulse trained by a genetic algorithm then creates the initial superposition of computing states on the ground state surface, and cycles population between them and the gateway state to perform the computation. The ground state vibrational levels of $SCCl_2$ and transition moments (ref. [21]) from which computing states are drawn are shown as blue/gray sticks, whose height indicates the transition dipole moment to/from the gateway state. The 16 states for the SHOR simulation from table 1 are identified by small circles; the computation also propagates the other states shown. The red/light gray Gaussians indicate the unshaped input pulse width for 2 qubit and 4 qubit simulations. At time t_f, the coherent superposition of computing states is projected onto the $1^1 2^1 4^1$ vibrational level at 20,085 cm^{-1} of the $\tilde{A}$ electronic state, separated by at least ±180 cm^{-1} from other strongly absorbing states. Fluorescence then monitors the relative phases and populations of the vibrational wave packet via quantum beats.

Figure 2: Optimized fidelity for a complete set of computational gates using thiophosgene spectral parameters: (a) Phase of π; (b) Toffoli; (c) Hadamard; (d) CNOT. Readout occurs at about 27 ps, as indicated by the dotted vertical line. The bandwidth of the Gaussian input pulse to the pulse shaper is shown in figure 1.

Figure 3: Fidelities for a two-qubit CNOT operator pulse acting on the three input states A-C in eq. (4), using the training set in eq. (3). These are worst-case entangled qubits. Similar performance is obtained for random component input vectors.

Figure 4: (Web color) The fidelity vs. time trace for the full phase estimation procedure from Shor's Algorithm (left, $M = 1024$ pixels). Above the fidelity is shown the windowed Fourier transform of the optimal computing pulse. The contour scale is from red (light gray) to blue (dark grey) from relative amplitudes 0 to 1.

Figure 5: Power fluctuations may come from shot-to-shot intensity variations, the varying position of molecules along the spatial profile of the laser, or the orientation of the target molecule with respect to the polarization axis of the laser (see also figure 6). At right, a CNOT shaper mask was optimized for three cases of laser power simultaneously (100% of maximum, 75% and 50%) and the resulting mask was tested for two intermediate cases (87.5% and 62.5%).

Figure 6: (Web color) Fidelity and windowed Fourier transform of the control pulse optimized for the CNOT gate as in figure 2, but with the rotational ladders included up to $J = 5$. The contour scale is from red (light gray) to blue (dark grey) from relative amplitudes 0 to 1.

Figure 7: (Web Color) CNOT fidelity at readout ($t = 27$ ps) for successive groups of four vibrational levels in the thiophosgene spectrum, arranged by center frequency. The maximum of the unshaped pulse envelope was moved to the center frequency of each group before optimization.

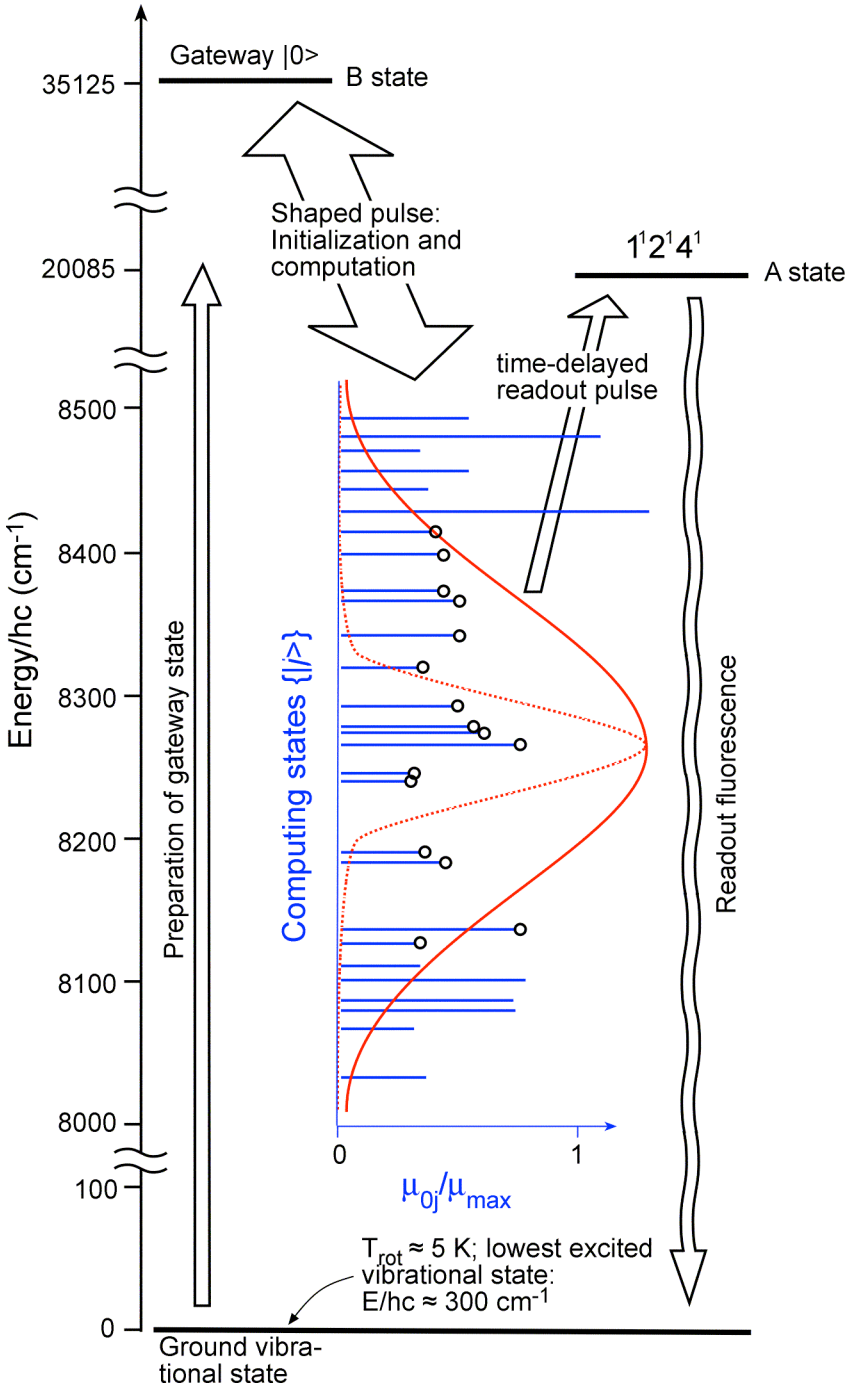

Figure 1, Weidinger & Gruebele
(single column format, web color)

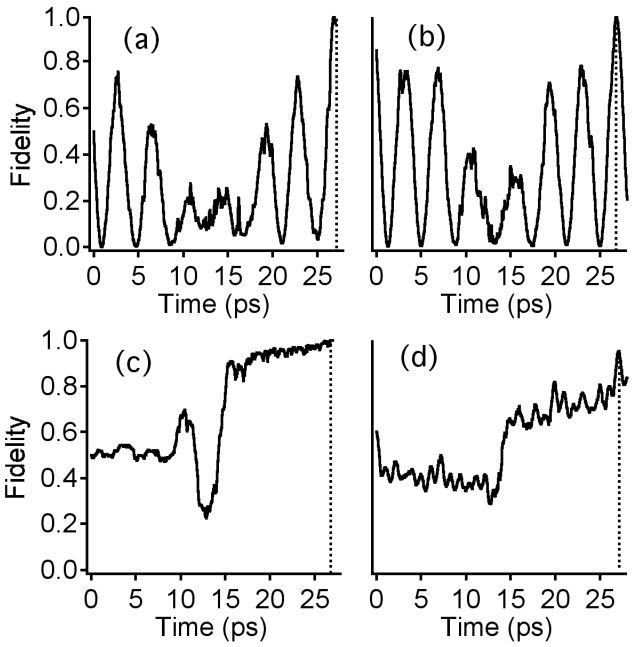

Figure 2, Weidinger & Gruebele
(single column format)

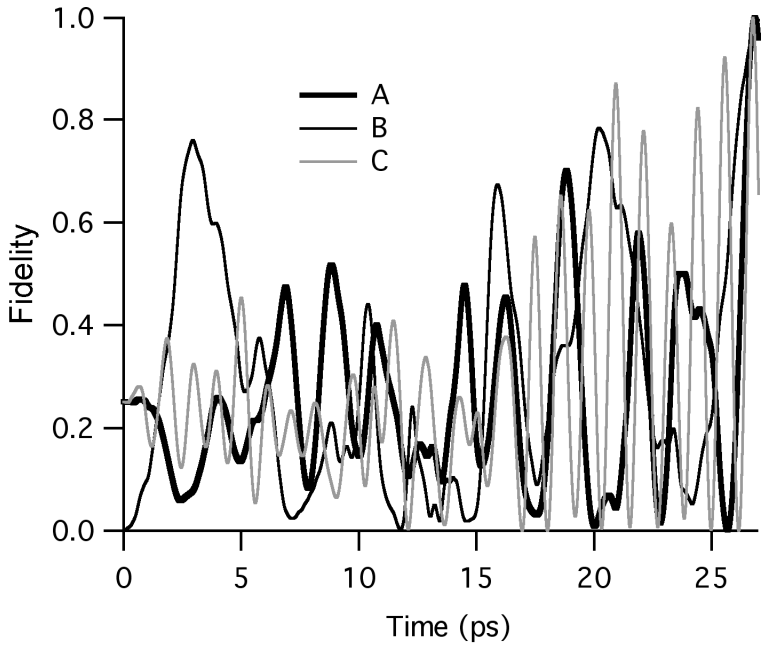

Figure 3, Weidinger & Gruebele
(single column format)

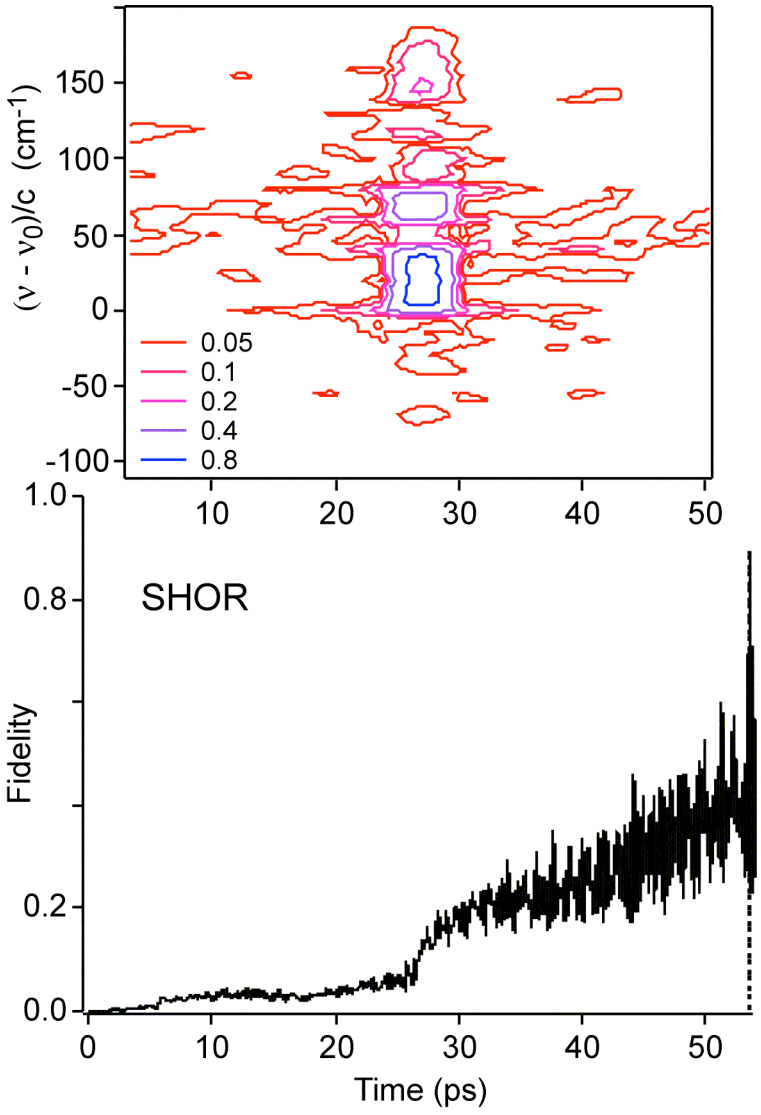

Figure 4, Weidinger & Gruebele
(Web color, single column format)

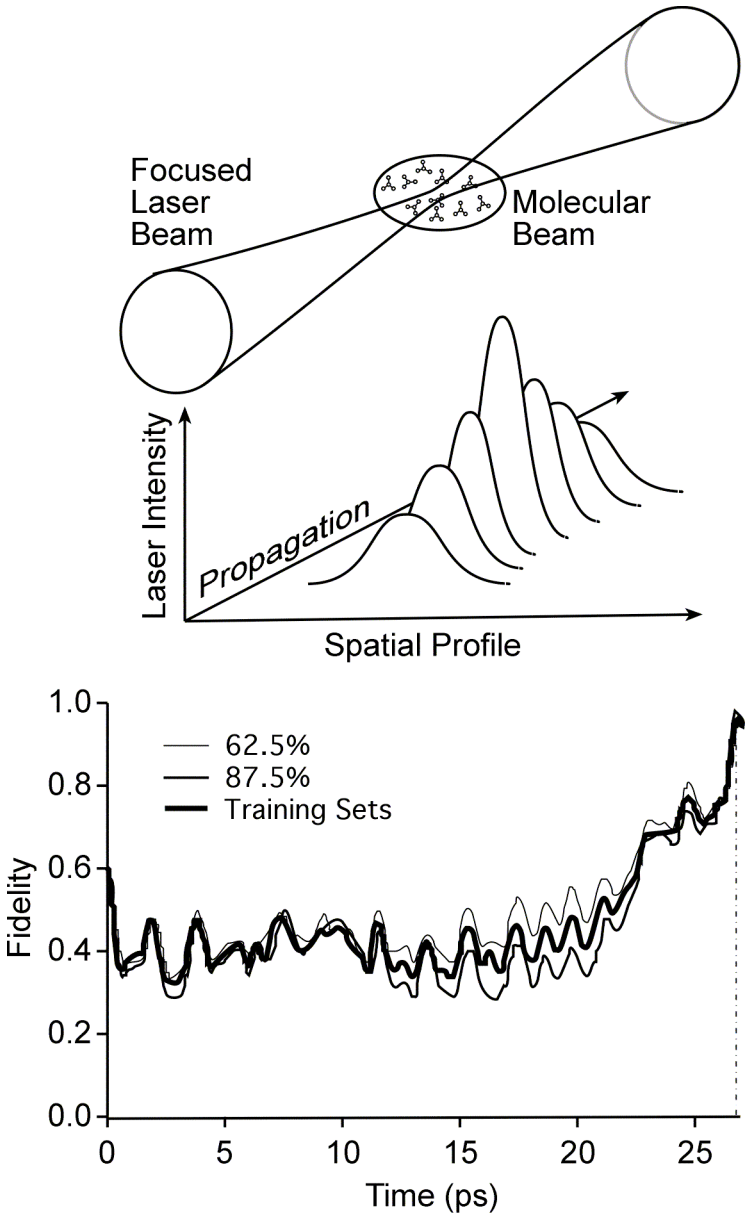

Figure 5, Weidinger & Gruebele
(single column format)

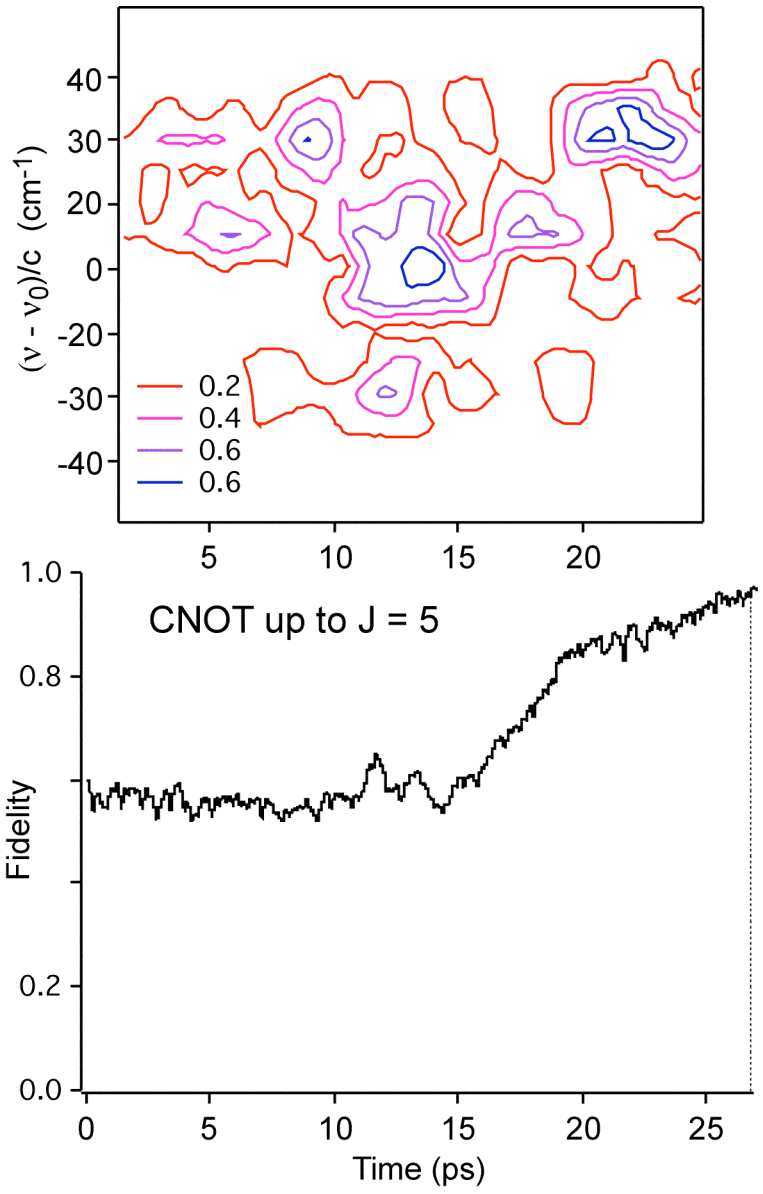

Figure 6, Weidinger & Gruebele
(single column format, web color)

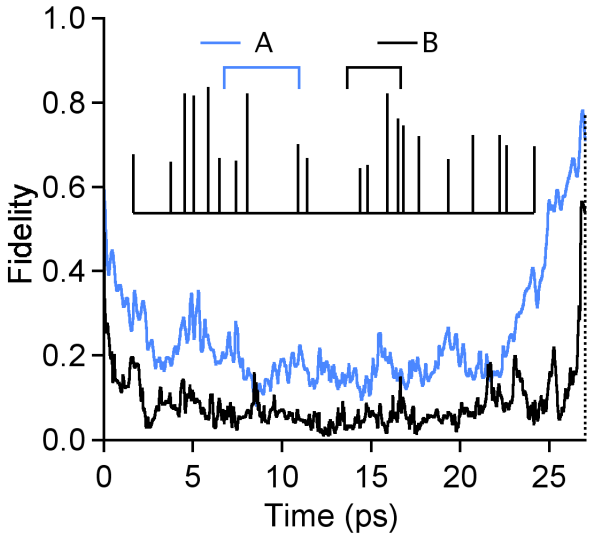

Figure 7, Weidinger & Gruebele
(single column format, web color)